Improved kinetic model of hydrogen absorption and desorption in titanium with subsurface transport

Yuta Shimohata, Yoshiki Hamamoto, Kengo Nishi, and Katsuaki Tanabe*

Department of Chemical Engineering, Kyoto University, Nishikyo, Kyoto 615-8510, Japan

*E-mail: tanabe@cheme.kyoto-u.ac.jp

Abstract

We improve our previous kinetic model of hydrogen transport in Ti [Y. Hamamoto *et al*., Nucl. Mater. Energy 23 (2020) 100751]. The model becomes applicable to both the directional processes of absorption and desorption. The limitation in the covered range of hydrogen molar fraction, previously up to 1 mol-H/mol-Ti, is dissolved. The numerical calculations based on the model with a single set of kinetic parameters closely reproduce a series of experimental hydrogen absorption and desorption data for various temperatures, and thus verify the validity of the model.

Keywords

Hydride; Adsorption; Diffusion; Hydrogen storage; Nuclear reactor; Fusion reactor

1. Introduction

Ti and its hydride are promising for use in applications including hydrogen storage [1–5] and in nuclear reactors [6–9]. Understanding the hydrogenation and dehydrogenation processes of Ti is important for the design in each application, and therefore the kinetics in the hydrogen–Ti system have been investigated [10,11]. Ti is used, for example, in the condenser tubes in nuclear reactors because of its high mechanical robustness and corrosion resistance against seawater [6,12]. Ti-based alloys and hydrides are expected to be used as a reactor component, coolant additive, and radiation shield, in nuclear fusion applications [9]. Ti is also promising to be used as a particulate additive in molten-salt blankets for tritium absorption and transportation in nuclear fusion reactors [13,14]. Such Ti particles can also suppress the corrosion of the tubes in the fusion reactor by sacrificially reacting with the corrosive HF and F species [15]. In addition, Ti is used as a dopant at the surface of lightweight hydrogen-storage materials with low surface activity, such as alkali metal aluminum hydrides, to increase the absorption and desorption velocity [16].

However, hydrogen absorption in Ti installed in operating environments in the presence of hydrogen can cause mechanical embrittlement to generate cracks and blisters in the equipment [17]. The sources of hydrogen in nuclear reactors include the dissolved hydrogen present in the cooling water or vapor, and the radiation-induced decomposition of water. Embrittlement of the constructive materials in nuclear power plants potentially induces disasters, such as radioactive leakage and hydrogen explosion. Hence, understanding and then controlling the hydrogen absorption process in metallic components are highly demanded for the prevention of hydrogen embrittlement. Absorption and desorption of hydrogen isotopes in the plasma facing walls of nuclear

fusion reactors are also important in view of embrittlement and undesirable hydrogen isotope emission to the plasma core that would negatively affect the reaction. Nevertheless, the kinetics of hydrogen transport in metals, particularly around the surface, have not been completely explained yet [18]. Previously, we developed a kinetic model of hydrogen absorption in Ti [19]. However, for hydrogen desorption from Ti, the model did not sufficiently reproduce experimental data, and therefore its applicability was limited to the absorption process. In addition, the applicability of the model was also limited to the conditions where the hydrogen molar fraction (mol-H/mol-Ti) is sufficiently lower than unity, because of the way we defined the surface coverage parameter. In the present study, we develop a single kinetic model of hydrogen transport in Ti applicable to both the directional processes of absorption and desorption, and without a limitation of the hydrogen molar fraction.

2. Theory and calculation methods

Table 1 lists the symbols used in the formulation. The fundamental concept of the numerical model of hydrogen absorption is described in Ref. 19 and schematically depicted in Fig. 1. The hydrogen mass balances are formulated as

$$X_{max} N_s \frac{d\theta}{dt} = J_{ads} - J_{des} - J_{sb} + J_{bs}, \qquad (1)$$

$$X_{max} N_s \frac{d\theta_{ss}}{dt} = J_{sb} - J_{bs} - J_{dif}\Big|_{subsurface}, \qquad (2)$$

$$\frac{N_b V_b}{A}\frac{dX}{dt} = J_{sb} - J_{bs} . \qquad (3)$$

X_{max} is the maximum hydrogen molar fraction, to be discussed later in this section. N_s is the molar density of Ti per surface area. θ is the fractional coverage, or occupancy, of hydrogen atoms at the surface. J_{ads} and J_{des} are the hydrogen fluxes for the surface adsorption and desorption processes, respectively. J_{sb} and J_{bs} are the hydrogen fluxes for the inward and outward subsurface transport, respectively. θ_{ss} is the fractional coverage of hydrogen atoms at the subsurface. J_{dif} is the hydrogen flux for the diffusion in the bulk region. N_b is the molar density of Ti per volume. V_b and A are the volume and surface area of Ti, respectively. X [mol-H/mol-Ti] is the hydrogen molar fraction in Ti. The values of N_s and N_b are calculated by

$$N_s = \frac{\left(N_A N_b\right)^{\frac{2}{3}}}{N_A} , \qquad (4)$$

$$N_b = \frac{\rho}{M} , \qquad (5)$$

where N_A is the Avogadro constant, ρ is the mass density of Ti, and M is the molar mass of Ti. Consequently, N_s and N_b are 2.16×10^{-5} mol·m^{-2} and 9.4×10^{4} mol·m^{-3}, respectively. The values of J_{ads}, J_{des} [11], J_{sb}, J_{bs} [20], and J_{dif} are determined by

$$J_{ads} = 2S_0\left(1-\theta\right)^2 \frac{P_{H_2}}{\sqrt{2\pi M_{H_2} RT_g}}, \qquad (6)$$

$$J_{des} = k_{des}{}^0 \theta^2 \exp\left(-\frac{E_{des}}{RT_s}\right), \qquad (7)$$

$$J_{sb} = k_{sb}{}^0 X_{max} N_s \theta \left(1-\theta_{ss}\right) \exp\left(-\frac{E_{sb}}{RT_s}\right), \qquad (8)$$

$$J_{bs} = k_{bs}{}^0 X_{max} N_s \theta_{ss} \left(1-\theta\right) \exp\left(-\frac{E_{bs}}{RT_s}\right), \qquad (9)$$

$$J_{dif} = D_H{}^0 \frac{\partial C\left(z,t\right)}{\partial \mathrm{z}} \exp\left(-\frac{E_{dif}}{RT_s}\right). \qquad (10)$$

S_0 is the sticking coefficient at zero coverage of hydrogen atoms onto the surface of Ti. P_{H2} and M_{H2} are the partial pressure and molar mass of hydrogen, respectively. R is the ideal gas constant. T_g and T_s are the absolute temperature of the gas and solid phases, respectively. $k_{des}{}^0$ (1.08×10^8 mol·m^{-2}·s^{-1} [11]), $k_{sb}{}^0$, and $k_{bs}{}^0$ are the frequency factors for the surface desorption, and the inward and outward subsurface transport of hydrogen atoms, respectively. E_{des} (1.17×10^5 J·mol^{-1} [11]), E_{sb}, E_{bs}, and E_{dif} (5.3×10^4 J·mol^{-1} [21]) are the activation energy values of hydrogen for the surface desorption, inward and outward subsurface transport, and diffusion in the bulk region, respectively. $D_H{}^0$ (9.0×10^{-7} m^2·s^{-1}

[21]) is the prefactor of the diffusion coefficient of hydrogen. C is the local concentration of hydrogen in the bulk. S_0 is unitless for Eq. 6 in the SI unit system and given by

$$S_0 = 0.0143 \exp\left(-\frac{E_{S_0}}{RT_s}\right), \qquad (11)$$

where E_{S0} (-1.99×10^3 J·mol^{-1} [11,22]) is the (regressive) activation energy value for the initial chemisorption [11,22]. The value of P_{H2} is calculated, by the ideal gas law, as

$$P_{H_2} = \left\{\frac{P_0 V_{ch}}{RT_0} + \frac{(X_0 - X)n_{Ti}}{2}\right\}\frac{RT_g}{V_{ch}}, \qquad (12)$$

P_0 is the initial hydrogen pressure. V_{ch}, is the chamber volume. T_0 is the initial temperature of the gas phase. X_0 is the initial hydrogen molar fraction in Ti. n_{Ti} is the number of moles of Ti. By balancing Eqs. 6 and 7, θ can be determined as

$$\theta = \frac{\sqrt{\alpha}}{1+\sqrt{\alpha}}, \qquad (13)$$

where

$$\alpha = \frac{2S_0 P_{H_2}}{k_{des}{}^0 \exp\left(-\frac{E_{des}}{RT_s}\right)\sqrt{2\pi M_{H_2} RT_g}}, \qquad (14)$$

under the assumption that hydrogen adsorption and desorption on the surface of Ti are in equilibrium [11,23,24] because of the high surface activity of Ti. We calculate θ by Eqs. 13 and 14, instead of Eq. 1, for the convenience in parameter fitting. Then, Eqs. 2 and 3 are numerically solved by the finite-difference, forward Euler method, with the update of $C(z)$ for each time step, to determine $X(t)$. The shape of Ti is assumed to be a two-dimensional layer with a finite thickness and an infinite area, and the hydrogen transport solely in the direction of the layer thickness is accounted for, in the present study. The symmetric boundary condition is employed at the central plane of Ti, $z = 0$. This setting is equivalent to the situation that there is no hydrogen flux across the central plane. Hydrogen absorption and desorption from the two outer surfaces of Ti are thus simulated. The values of k_{sb}^{0}, k_{bs}^{0}, E_{sb}, and E_{bs} are to be determined by numerical fitting. As observed in the form of Eqs. 6, 8, and 9, θ and θ_{ss} are defined in the range below unity. In our previous model [19], we did not account for X_{max}, or X_{max} was treated to be unity. Because of the abovementioned definition of N_s, the situation $\theta = \theta_{ss} = 1$ corresponded to the one $X = 1$ in our previous model. Therefore, the applicability of the model was limited to the conditions where X is lower than unity. In the present study, we have incorporated X_{max} into the model to remove the artificial limitation. To determine the value of X_{max}, we account for the lattice structures of Ti. As depicted in Fig. 2, the α phase of Ti takes the hexagonal close-packed structure with the number of Ti atoms of 2 in a unit cell. H atoms can occupy a half of the tetrahedral sites at most, because of the site blocking effect. In this situation, the number of H atoms in a unit cell is also 2, resulting in $X_{max} = 1$. The β phase of Ti takes the body-centered cubic structure with the number of Ti atoms of 2 in a unit cell. H atoms can occupy a half of the tetrahedral sites at most, again because of the site blocking effect. In

this situation, the number of H atoms in a unit cell is 6, resulting in X_{max} = 3. The δ phase of Ti takes the face-centered cubic structure with the number of Ti atoms of 4 in a unit cell. H atoms can occupy all of the tetrahedral sites at most. In this situation, the number of H atoms in a unit cell is 8, resulting in X_{max} = 2. Therefore, we set X_{max} to be 3 as the maximum possible hydrogen molar fraction, which may be consistent with the common view for Ti in the community [25–27]. In contrast to the modification of N_s into $X_{max}N_s$, N_b does not need to be changed because X varies up to X_{max}, but is not defined in the range below unity, unlikely to θ and θ_{ss}. As another modification of the model, we assumed that T_g and T_s were always equal to each other, and therefore treated them as a single, common variable in our previous model [19]. In contrast, we distinguish them for generality in the present model.

3. Results and discussion

By using a series of experimental results, we prove the validity of the hydrogen transport model. The experimental data in Ref. 10 is employed. The conditions of the experiments were: V_b = 1.3 cm × 1.0 cm × 1.0 mm, P_0 = 1.3 × 10^4 Pa, V_{ch} is unknown [10]. To estimate the value of V_{ch}, we use the relation between the equilibrium hydrogen pressure against the β phase of Ti, $P_{\beta\text{-}eq}$, and the equilibrium hydrogen molar fraction in Ti, X_{eq}, reported in Ref. 26:

$$P_{\beta-eq}[Pa] = 101325 \exp\left\{15.84 + 0.7X_{eq} + 2\ln\left(\frac{X_{eq}}{2-X_{eq}}\right) - \frac{1.6\times10^4}{T_s[K]}\right\} \quad (15).$$

Through Eqs. 12, 15, and the X_{eq} values observed in the experimental data of Ref. 10 in the

regime of β phase, we can reasonably estimate V_{ch}, as 2.95×10^{-3} m^3. We assumed that T_g is equal to T_s for the calculations for the hydrogen absorption process in this study, as we did in Ref. 19. Figure 3 plots the hydrogen absorption curves at different temperatures for the experiments in Ref. 10, and our numerical simulation results. The fitting parameters k_{sb}^0, k_{bs}^0, E_{sb}, and E_{bs} are determined as 1.16×10^{11} s^{-1}, 3.24×10^9 s^{-1}, 1.18×10^5 J·mol^{-1}, and 8.50×10^4 J·mol^{-1}, respectively. Table 2 summarizes the values of the kinetic parameters used in this study. Ref. 10 reported overall activation energies for absorption and desorption of 7.4×10^4 J·mol^{-1} and 2.5×10^4 J·mol^{-1}, respectively. Ref. 11 reported E_{sb} and E_{bs} of 1.33×10^5 J·mol^{-1} (for $\theta = 1$) and 1.35×10^5 J·mol^{-1}, respectively. Assuming a subsurface-control situation for Ref. 10, the values of our E_{sb} and E_{bs} lie in the middle of those of Refs. 10 and 11. The calculation results, with a single set of kinetic parameters, closely reproduce a series of experimental results for various temperatures, as observed in Fig. 3. The degree of fitting to the same set of experimental data is higher than the case of our previous model [19].

To demonstrate the significance of the introduction of X_{max} in our present model and to check the validity of the model in the high-X regime, we plot in Fig. 4 the hydrogen absorption curves for a Ti layer with a thickness of 1 mm under a constant hydrogen pressure of 1 atm at 900 K, calculated by the present and previous models. As a reference, the phase diagram of the hydrogen–Ti system in Ref. 26 presents that X_{eq} for a hydrogen pressure of 1 atm at 900 K is 1.6. As observed in Fig. 4, X_{eq} is calculated to be 0.90 for the previous model, and thus inconsistent with the literature value, due to the formulation of the previous model corresponding to the situation $X_{max} = 1$. Even for a hydrogen pressure of 100 atm, X_{eq} is calculated to be 0.996. In contrast, X_{eq} is calculated to be 1.7 for the

present model, as observed in Fig. 4. Thus, our present model approximately reproduces the literature value of X_{eq} also in the high-X region, which would not have been realized by our previous model.

Figure 5 plots the hydrogen desorption curves at different temperatures for the experiments in Ref. 10, and our numerical simulation results with the same single set of parameter values of k_{ads}^0, k_{des}^0, E_{ads}, and E_{des} as those for Fig. 3. For the calculations for the hydrogen desorption process in this study, we assume T_g to be 300 K accounting for the rapid decrease in the temperature of the desorbed hydrogen gas owing to the adiabatic expansion. The experimental desorption curves are thus satisfactorily reproduced for all the temperatures, in contrast to the poor fit by our previous model [19]. The discrepancy between the experimental data and the calculation curves around the initial stage might be attributed to the unknown heating period to the set temperature after the transportation of the Ti sample to the hot zone at t = 0 in Ref. 10, while the calculation assumed a constant T_s. Importantly, this data reproduction is accomplished with the same sets of formulae and parameters as those for the hydrogen absorption process, and therefore our single model is applicable to both absorption and desorption.

After we verified the validity of the hydrogen absorption and desorption model and determined the values of the kinetic parameters, we carry out case studies to exhibit the practicality of the model. Ti was expected to be used for the first wall in nuclear fusion reactors [28,29], as well as the present use as a material for condenser tubes in nuclear reactors [6,12]. Whilst, Ti can be considered not be very effective as a first wall material, as its tritium inventory would be too high to be accepted from viewpoints of fuel cycle feasibility and fusion reactor safety. Absorption of hydrogen isotopes into such materials causes their hydrogen embrittlement [30]. In this context, we analyze the dependence of the

hydrogen absorption rate on the thickness of the Ti layer. Firstly, we plot in Fig. 6 the calculated dependence of X_{eq} on the hydrogen pressure at 550 ºC, as an assumed surface temperature of the first wall [31]. Note that X_{eq} does not depend on the thickness of the Ti layer, while the hydrogen absorption rate does. For this calculation and hereafter, we allow for the hydrogen transport only through one surface of the Ti layer and the other surface is set to be impermeable, to correspond to the practical situations. As the hydrogen molar fraction for the onset of hydrogen embrittlement in Ti lies on the order of 100 ppm (1 ppm = 1×10^{-6} mol-H/mol-Ti), we assume the embrittlement threshold as X = 100 ppm in this case study. Under this assumption, from the result of Fig. 6, hydrogen embrittlement can occur for the hydrogen pressure higher than 10^{-1} Pa, which is, incidentally, slightly below the partial pressure of hydrogen in the ambient air. Figure 7 presents the calculated hydrogen absorption curves for Ti layers with various thicknesses under a constant hydrogen pressure of 1.0×10^{-1} Pa at 550 ºC. The tendency that the period to reach the embrittlement threshold becomes longer as the Ti thickness becomes larger is observed. We summarize in Fig. 8 the dependence of the period to reach the embrittlement threshold, X = 100 ppm, on the Ti thickness under a constant hydrogen pressure of 1.0×10^{-1} Pa at 550 ºC, extracted from the calculated hydrogen absorption curves for various Ti thicknesses. From such a series of numerical simulations, one can determine for example the frequency of the equipment maintenance treatment, such as material replacement or bake-out, from the thickness of the Ti layer, and vice versa.

As a case study using our model for the hydrogen desorption process, we employ the experimental data in Ref. 28. They measured the deuterium desorption rate from a Ti layer deposited on a substrate, as a fundamental investigation for the first wall in nuclear fusion reactors. The conditions of the experiments were as follows: The thickness of the Ti layer

was 100 nm. The initial deuterium density contained in the Ti layer was 3.3×10^{17} D/cm^2. The sample was heated at a rate of 30 K/min in a vacuumed chamber. During the heating process, the desorption rate of deuterium gas was measured by using a quadrupole mass spectrometer. The pressure in the chamber is not described in the literature, but we assumed the deuterium pressure during the experiment to be 1.0×10^{-8} Pa in our calculations. Figure 9 plots the evolution of the deuterium desorption rate on the Ti temperature in the experiment [28], and our calculation results. Relative to our calculated curve with the original set of kinetic parameters, the one with modified E_{des} into 2.10×10^5 J·mol^{-1} and E_{S0} into 90.0 J·mol^{-1} provided a better reproduction of the experimental data. This modification of E_{des} and E_{S0} accounted for the potential formation of a native oxide layer on the Ti layer, and was carried out by numerical fitting. In this manner, our model can also be used for numerical simulations for the desorption process of hydrogen isotopes. The difference between the experimental and calculated curves in Fig. 9 might be attributed to possible retardation in the heat transfer in the Ti sample from the heater or in the detection by the mass spectrometer. The difference in the kinetic properties between hydrogen (our model) and deuterium (the experiment) might also influence. Employment of the kinetic parameter values for hydrogen isotopes into our model would be preferable for the precision of numerical simulations in the nuclear field.

4. Conclusions

In this study, we improved our previous kinetic model of hydrogen transport in Ti. Consequently, the model became applicable to both the directional processes of absorption and desorption. The limitation in the covered range of X, which previously had to be sufficiently lower than 1 mol-H/mol-Ti, was removed. The numerical calculations based on

the model satisfactorily reproduced the experimental hydrogen absorption and desorption data taken at various temperatures, with a single set of kinetic parameters, and thus demonstrated the validity of the model. Case studies for hydrogen absorption and desorption in relation to the first wall in nuclear fusion reactors were carried out to demonstrate the usefulness of our numerical model. Practically, at the plasma facing wall of a fusion reactor, the effect of hydrogen isotope gas may be smaller than that of hydrogen isotope incident from the plasma. In such a case, model/parameter modifications are required to reflect the characteristics of the hydrogen isotope plasmas. Our renewed hydrogen transport model with enhanced applicability could be a useful simulation tool.

Declaration of competing interest

The authors declare that there is no conflict of interests.

Acknowledgements

This work was financially supported by the Japan Society for the Promotion of Science.

References

[1] D.H. Bradhurst, P.M. Heuer, G.Z.A. Stolarski, Hydrogen-production and storage using titanium electrodes and metal-hydrides, Int. J. Hydrogen Energy 8 (1983) 85–90, https://doi.org/10.1016/0360-3199(83)90090-3.

[2] C.S. Wang, Y.Q. Lei, Q.D. Wang, Effects of Nb and Pd on the electrochemical properties of a Ti-Ni hydrogen-storage electrode, J. Power Sources 70 (1998) 222–227, https://doi.org/10.1016/S0378-7753(97)02674-8.

[3] K.F. Kelton, J.J. Hartzell, R.G. Hennig, V.T. Huett, A. Takasaki, Hydrogen storage in Ti-Zr and Ti-Hf-based quasicrystals, Phil. Mag. 86 (2006) 957–964, https://doi.org/10.1080/14786430500300173.

[4] C.G. Zhang, R.W. Zhang, Z.X. Wang, Z. Zhou, S.B. Zhang, Z.F. Chen, Ti-substituted boranes as hydrogen storage materials: A computational quest for ideal combination of stable electronic structure and optimal hydrogen uptake, Chem. A Euro. J. 15 (2009) 5910–5919, https://doi.org/10.1002/chem.200900172.

[5] R. Kondo, S. Nakamichi, R. Azuma, Y. Takahashi, Y. Obora, H.T. Takeshita, Surface properties of air-exposed α-Ti-Pd alloys via XPS and cross-coupling reaction, Mater. Trans. 59 (2018) 1911–1914, https://doi.org/10.2320/matertrans.M2018240.

[6] M. Hedstroem, I. Multer, Titanium condenser – Optimal solution for nuclear-power stations with seawater cooling, Trans. Am. Nucl. Soc. 31 (1979) 66–67.

[7] E.A. Marquis, J.M. Hyde, D.W. Saxey, S. Lozano-Perez, V. de Castro, D. Hudson, C.A. Williams, S. Humphry-Baker, G.D.W. Smith, Nuclear reactor materials at the atomic scale, Mater. Today 12 (2009) 30–37, https://doi.org/10.1016/S1369-7021(09)70296-2.

[8] T. Allen, J. Busby, M. Meyer, D. Petti, Materials challenges for nuclear systems, Mater.

Today 13 (2010) 14–23, https://doi.org/10.1016/S1369-7021(10)70220-0.

[9] T. Tanaka, H. Muta, Y. Hishinuma, H. Tamura, T. Muroga, A. Sagara, Applicability of hydride materials for radiation shielding in helical reactor FFHR-D1, Fusion Sci. Technol. 68 (2015) 705–710, https://doi.org/10.13182/FST15-110.

[10] Y. Hirooka, M. Miyake, T. Sano, A study of hydrogen absorption and desorption by titanium, J. Nucl. Mater. 96 (1981) 227–232, https://doi.org/10.1016/0022-3115(81)90566-3.

[11] C.C. Brown, R.E. Buxbaum, Kinetics of hydrogen absorption in alpha titanium, Metallurgical Trans. A 19A (1988) 1425–1427, https://doi.org/10.1007/BF02674016.

[12] S. Anandan, R. Rajesh, K. Ganesh, A study of the condenser in nuclear power plants, Int. J. ChemTech Res. 10 (2017) 9–16, http://www.sphinxsai.com/2017/ch_vol10_no14/1/(09-16)V10N14CT.pdf.

[13] T. Watanabe, A. Sagara, J. Yagi, T. Tsujimura, G. Yamazaki, K. Kumagai, T. Tanaka, Hydrogen recovery from metal particle dispersed salt by selective microwave heating, Fusion Eng. Des. 136 (2018) 1396–1399, https://doi.org/10.1016/j.fusengdes.2018.05.021.

[14] K. Tanabe, Selective electromagnetic induction heating of metal particles in molten salt for tritium extraction: A systematic numerical investigation, Fusion Eng. Des. 163 (2021) 112177, https://doi.org/10.1016/j.fusengdes.2020.112177.

[15] G. Yamazaki, J. Yagi, T. Tanaka, T. Watanabe, A. Sagara, Sacrificial effect of titanium powder on the corrosion by hydrogen fluoride in LiF-NaF-KF, Fusion Eng. Des. 136 (2018) 394–397, https://doi.org/10.1016/j.fusengdes.2018.02.054.

[16] B. Bogdanovic, M. Schwickardi, Ti-doped alkali metal aluminium hydrides as potential novel reversible hydrogen storage materials, J. Alloys Compd. 253 (1997) 1–9,

https://doi.org/10.1016/S0925-8388(96)03049-6.

[17] C.L. Briant, Z.F. Wang, N. Chollocoop, Hydrogen embrittlement of commercial purity titanium, Corrosion Sci. 44 (2002) 1875–1888, https://doi.org/10.1016/S0010-938X(01)00159-7.

[18] K. Fukutani, M. Wilde, S. Ogura, Nuclear dynamics and electronic effects of hydrogen on solid surfaces, Chem. Rec. 17 (2017) 233–249, https://doi.org/10.1002/tcr.201600077.

[19] Y. Hamamoto, T. Uchikoshi, K. Tanabe, Comprehensive modeling of hydrogen transport and accumulation in titanium and zirconium, Nucl. Mater. Energy 23 (2020) 100751, https://doi.org/10.1016/j.nme.2020.100751.

[20] S. Ono, T. Uchikoshi, Y. Hayashi, Y. Kitagawa, G. Yeh, E. Yamaguchi, K. Tanabe, A heterothermic kinetic model of hydrogen absorption in metals with subsurface transport, Metals 9 (2019) 1131, https://doi.org/10.3390/met9101131.

[21] G.W. Wille, J.W. Davis, Hydrogen in titanium alloys, US DOE Technical Reports (1981) DOE/ET/52039-2, https://doi.org/10.2172/6420120.

[22] D.J. Harra, Review of sticking coefficients and sorption capacities of gases on titanium films, J. Vac. Sci. Technol. 13 (1976) 471–474, https://doi.org/10.1116/1.568900.

[23] I. Ali-Khan, K.J. Dietz, F.G. Waelbroeck, P. Wienhold, The rate of hydrogen release out of clean metallic surfaces, J. Nucl. Mater. 76–77 (1978) 337–343, https://doi.org/10.1016/0022-3115(78)90167-8.

[24] T.L. Ward, T. Dao, Model of hydrogen permeation behavior in palladium membranes, J. Membr. Sci. 153 (1999) 211–231, https://doi.org/10.1016/S0376-7388(98)00256-7.

[25] P. Millenbach, M. Givon, The electrochemical formation of titanium hydride, J. Less Common Metals 87 (1982) 179–184, https://doi.org/10.1016/0022-5088(82)90086-8.

[26] W.-E. Wang, Thermodynamic evaluation of the titanium-hydrogen system, J. Alloys Compd. 238 (1996) 6–12, https://doi.org/10.1016/0925-8388(96)02264-5.

[27] Y. Fukai, The Metal–Hydrogen System: Basic Bulk Properties, 2nd ed., Springer, Berlin (2005) p. 124.

[28] T. Hino, Y. Hashiba, Y. Yamauchi, Y. Hirohata, K. Nishimura, N. Ashikawa, S. Masuzaki, A. Sagara, N. Noda, N. Ohyabu, A. Komori, O. Motojima, Deuterium retention and desorption behavior of boron–titanium as first wall material of fusion experimental device, Fusion Eng. Des. 81 (2006) 127–131, https://doi.org/10.1016/j.fusengdes.2005.05.003.

[29] A. Tankut, K.E. Miller, F.S. Ohuchi, PVD Ti-films for plasma-facing first walls, Part I: Characterization of surface chemistry during H_2 and O_2 exposure, J. Nucl. Mater. 433 (2013) 404–411, https://doi.org/10.1016/j.jnucmat.2012.10.005.

[30] O.V. Ogorodnikova, X. Raepsaet, M.A. Fütterer, Tritium permeation through the first wall of the EU-HCPB blanket, Fusion Eng. Des. 49–50 (2000) 921–926, https://doi.org/10.1016/S0920-3796(00)00339-2.

[31] L.M. Giancarli, M. Abdou, D.J. Campbell, V.A. Chuyanov, M.Y. Ahn, M. Enoeda, C. Pan, Y. Poitevin, E. Rajendra Kumar, I. Ricapito, Y. Strebkov, S. Suzuki, P.C. Wong, M. Zmitko, Overview of the ITER TBM Program, Fusion Eng. Des. 87 (2012) 395–402, https://doi.org/10.1016/j.fusengdes.2011.11.005.

Figure Captions

Table 1. List of the symbols, their definitions, and units used in the formulation.

Fig. 1. Conceptual schematic diagram of our calculation model for hydrogen absorption into Ti. J_{ads} and J_{des} are the hydrogen fluxes for the surface adsorption and desorption processes, respectively; J_{sb} and J_{bs} are the fluxes for the migration of hydrogen from the surface to the subsurface, and from the subsurface to the surface, respectively; J_{dif} is the hydrogen flux for diffusion in the bulk region; and θ and θ_{ss} are the fractional coverages at the surface and subsurface, respectively. Reprinted with permission from Ref. 19. Copyright 2020 Elsevier.

Fig. 2. Schematics of the lattice structures of Ti and the atomic sites. The mathematic formulae calculate the number of atoms in a unit cell. The mark * indicates the operation owing to the site blocking effect.

Fig. 3. Hydrogen absorption curves for Ti at different temperatures (marks: experimental results [10], lines: calculation results). The fitting parameters are $k_{sb}^{0} = 1.16 \times 10^{11}$ s^{-1}, $k_{bs}^{0} = 3.24 \times 10^{9}$ s^{-1}, $E_{sb} = 1.18 \times 10^{5}$ J·mol^{-1}, and $E_{bs} = 8.50 \times 10^{4}$ J·mol^{-1} for all the calculations.

Table 2. Summary of the values of the kinetic parameters and their references used in this study.

Fig. 4. Hydrogen absorption curves for a Ti layer with a thickness of 1 mm under a constant hydrogen pressure of 1 atm at 900 K, calculated by the present and previous models.

Fig. 5. Hydrogen desorption curves for Ti at different temperatures (marks: experimental results [10], lines: calculation results). The same single set of parameter values of k_{ads}^{0}, k_{des}^{0}, E_{ads}, and E_{des} as those for Fig. 2 is used for all the calculations.

Fig. 6. Calculated dependence of X_{eq} on the hydrogen pressure at 550 ºC.

Fig. 7. Calculated hydrogen absorption curves for Ti layers with various thicknesses under a constant hydrogen pressure of 1.0×10^{-1} Pa at 550 ºC.

Fig. 8. Dependence of the period to reach the embrittlement threshold, X = 100 ppm, on the Ti thickness under a constant hydrogen pressure of 1.0×10^{-1} Pa at 550 ºC.

Fig. 9. Evolution of the deuterium desorption rate on the Ti temperature in the experiment [28], and our calculation results with the original and modified kinetic parameters.

A	Surface area of Ti	[m^2]
C	Local concentration of hydrogen in the bulk	[mol m^{-3}]
D_H^0	Prefactor of diffusion coefficient of hydrogen	[m^2 s^{-1}]
E_{bs}	Activation energy for outward subsurface transport of hydrogen	[J mol^{-1}]
E_{des}	Activation energy for surface desorption of hydrogen	[J mol^{-1}]
E_{dif}	Activation energy for diffusion of hydrogen in the bulk region	[J mol^{-1}]
E_{sb}	Activation energy for inward subsurface transport of hydrogen	[J mol^{-1}]
E_{S0}	Activation energy for initial chemisorption	[J mol^{-1}]
J_{ads}	Hydrogen flux for surface adsorption	[mol m^{-2} s^{-1}]
J_{bs}	Hydrogen flux for outward subsurface transport	[mol m^{-2} s^{-1}]
J_{des}	Hydrogen flux for surface desorption	[mol m^{-2} s^{-1}]
J_{dif}	Hydrogen flux for diffusion in bulk region	[mol m^{-2} s^{-1}]
J_{sb}	Hydrogen flux for inward subsurface transport	[mol m^{-2} s^{-1}]
k_{bs}^0	Frequency factor for outward subsurface transport of hydrogen atoms	[s^{-1}]
k_{des}^0	Frequency factor for surface desorption of hydrogen atoms	[mol m^{-2} s^{-1}]
k_{sb}^0	Frequency factor for inward subsurface transport of hydrogen atoms	[s^{-1}]
M	Molar mass of Ti	[kg mol^{-1}]
M_{H2}	Molar mass of hydrogen	[kg mol^{-1}]
N_A	Avogadro constant	[mol^{-1}]
N_b	Molar density of Ti per volume	[mol m^{-3}]
N_s	Molar density of Ti per surface area	[mol m^{-2}]
n_{Ti}	Number of moles of Ti	[mol]
P_{H2}	Partial pressure of hydrogen	[Pa]
$P_{\beta\text{-}eq}$	Equilibrium hydrogen pressure against β phase of Ti	[Pa]
P_0	Initial hydrogen pressure	[Pa]
R	Ideal gas constant	[J mol^{-1} K^{-1}]
S_0	Sticking coefficient of hydrogen atoms onto Ti surface	[–]
t	Time	[s]
T_g	Absolute temperature of gas phase	[K]
T_s	Absolute temperature of solid phase	[K]
T_0	Initial temperature of gas phase	[K]
V_b	Volume of Ti	[m^3]
V_{ch}	Chamber volume	[m^3]
X	Hydrogen molar fraction in Ti	[–] (mol-H/mol-Ti)
X_{eq}	Equilibrium hydrogen molar fraction in Ti	[–] (mol-H/mol-Ti)
X_{max}	Maximum hydrogen molar fraction in Ti	[–] (mol-H/mol-Ti)
X_0	Initial hydrogen molar fraction in Ti	[–] (mol-H/mol-Ti)

θ	Fractional coverage of hydrogen atoms at Ti surface	[–]
θ_{ss}	Fractional coverage of hydrogen atoms at the subsurface	[–]
ρ	Mass density of Ti	[kg m^{-3}]

Table 1.

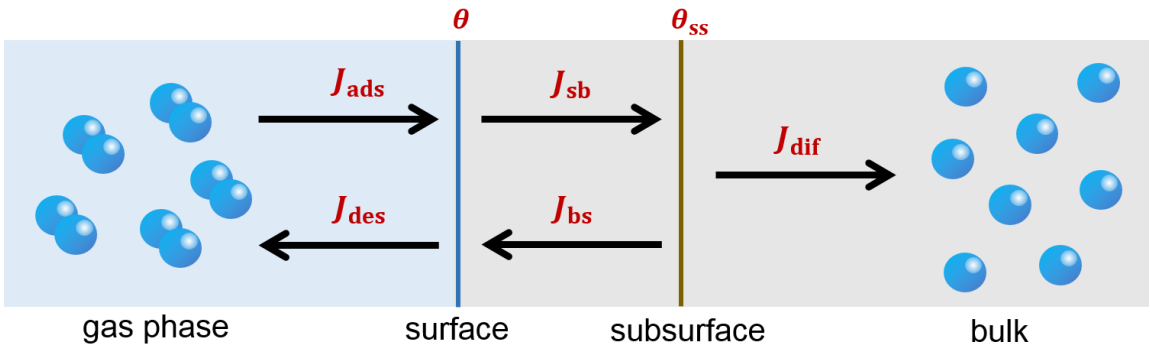
θ
θss
Jads
Jsb
Jdif
Jdes
Jbs
gas phase
surface
subsurface
bulk

Fig. 1.

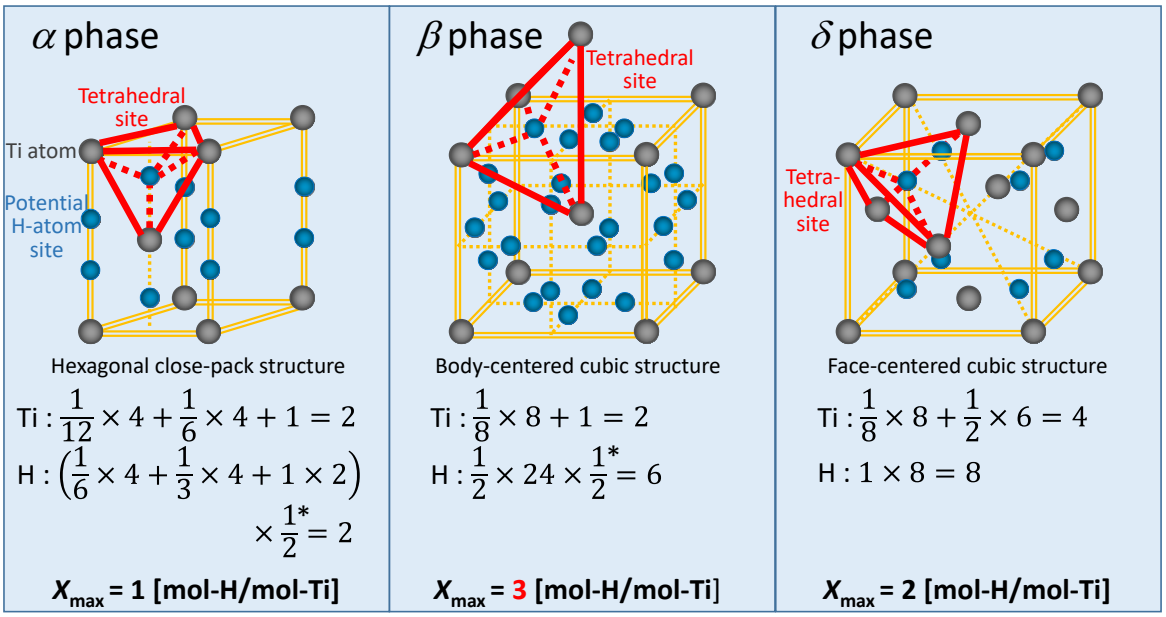
α phase
Tetrahedral site
Ti atom
Potential H-atom site
Hexagonal close-pack structure
$\mathrm{Ti}: \frac{1}{12} \times 4 + \frac{1}{6} \times 4 + 1 = 2$
$\mathrm{H}: \left(\frac{1}{6} \times 4 + \frac{1}{3} \times 4 + 1 \times 2\right) \times \frac{1^*}{2} = 2$
X_{max} = 1 [mol-H/mol-Ti]
β phase
Tetrahedral site
Body-centered cubic structure
$\mathrm{Ti}: \frac{1}{8} \times 8 + 1 = 2$
$\mathrm{H}: \frac{1}{2} \times 24 \times \frac{1^*}{2} = 6$
X_{max} = 3 [mol-H/mol-Ti]
δ phase
Tetra-hedral site
Face-centered cubic structure
$\mathrm{Ti}: \frac{1}{8} \times 8 + \frac{1}{2} \times 6 = 4$
$\mathrm{H}: 1 \times 8 = 8$
X_{max} = 2 [mol-H/mol-Ti]

Fig. 2.

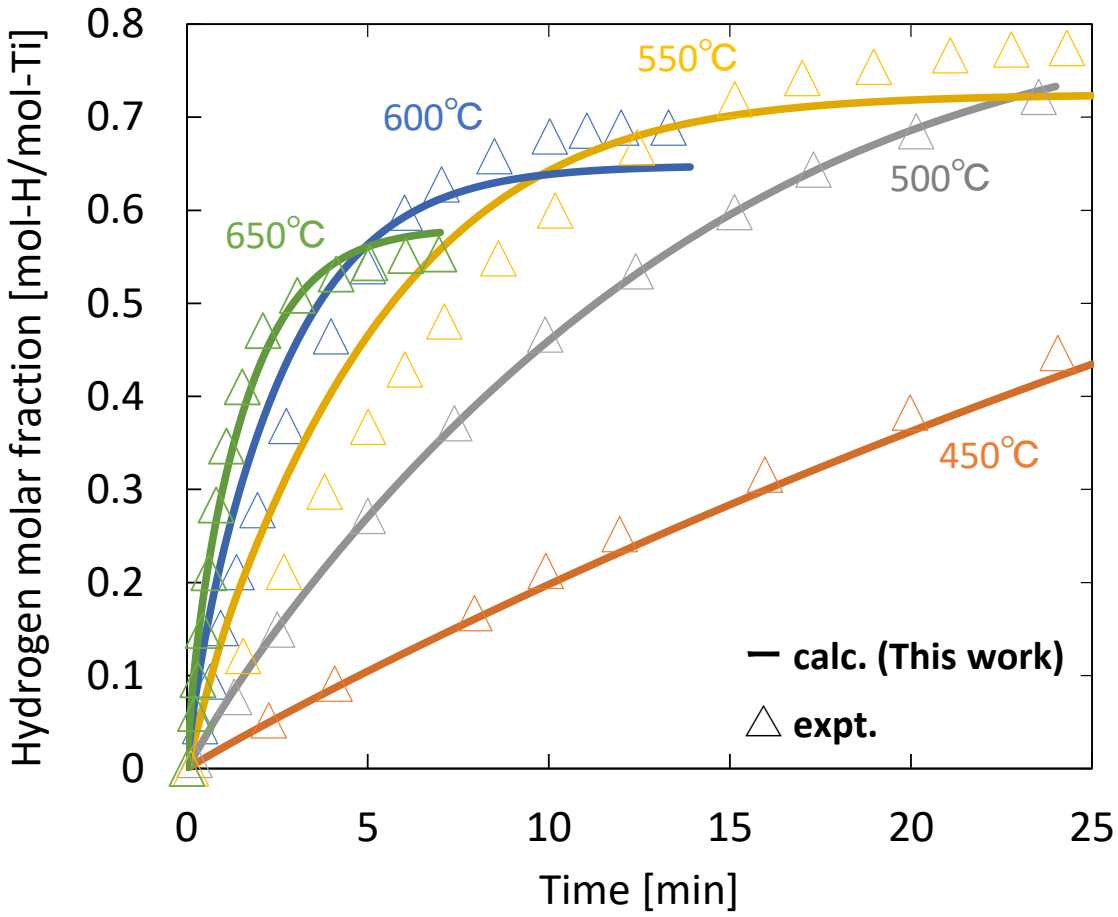
Hydrogen molar fraction [mol-H/mol-Ti]
0.8
0.7
0.6
0.5
0.4
0.3
0.2
0.1
0
0
5
10
15
20
25
Time [min]
550℃
600℃
650℃
500℃
450℃
calc. (This work)
expt.

Fig. 3.

D_H^0	9.0×10^{-7} m^2·s^{-1}	Ref. 21
E_{bs}	8.50×10^4 J·mol^{-1}	This work
E_{des}	1.17×10^5 J·mol^{-1}	Ref. 11
E_{dif}	5.3×10^4 J·mol^{-1}	Ref. 21
E_{sb}	1.18×10^5 J·mol^{-1}	This work
E_{S0}	-1.99×10^3 J·mol^{-1}	Refs. 11, 21
k_{bs}^0	3.24×10^9 s^{-1}	This work
k_{des}^0	1.08×10^8 mol·m^{-2}·s^{-1}	Ref. 11
k_{sb}^0	1.16×10^{11} s^{-1}	This work

Table 2.

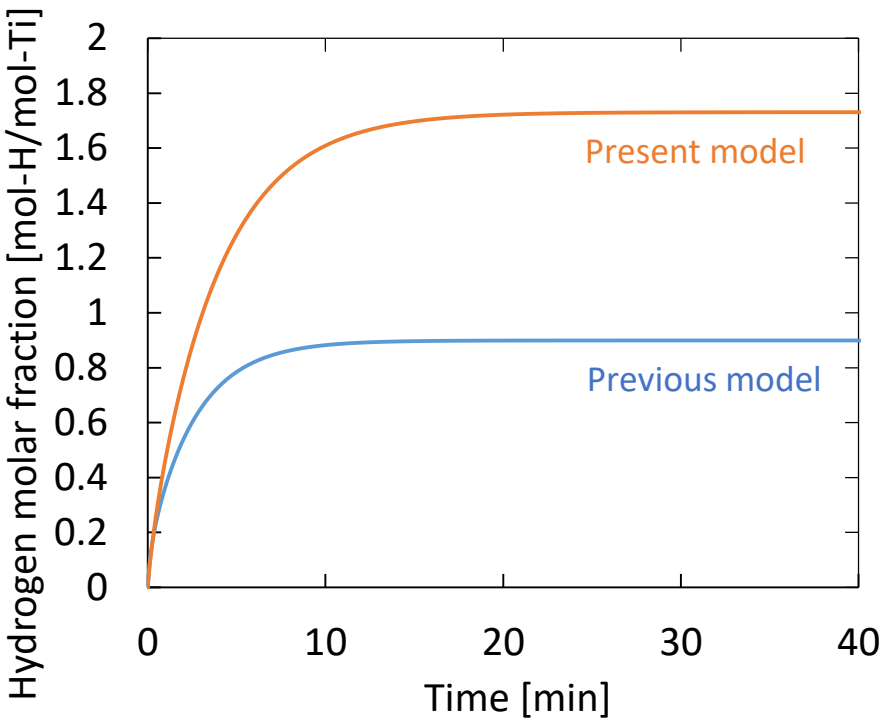
Hydrogen molar fraction [mol-H/mol-Ti]
2
1.8
1.6
1.4
1.2
1
0.8
0.6
0.4
0.2
0
0
10
20
30
40
Time [min]
Present model
Previous model

Fig. 4.

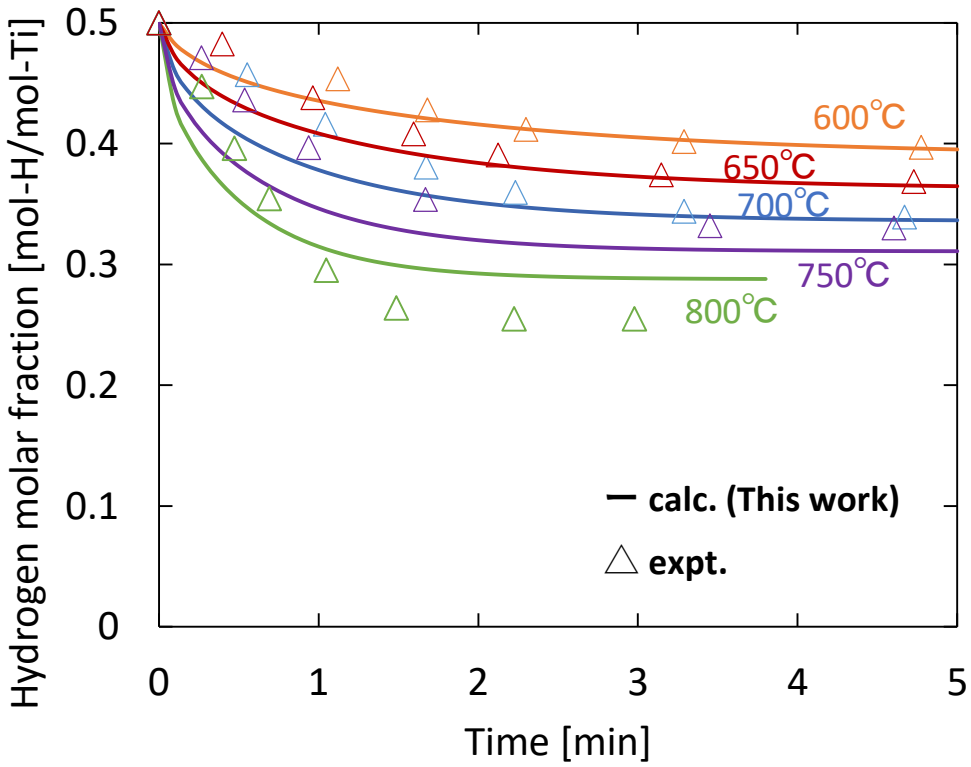
Hydrogen molar fraction [mol-H/mol-Ti]
0.5
0.4
0.3
0.2
0.1
0
0
1
2
3
4
5
Time [min]
600℃
650℃
700℃
750℃
800℃
calc. (This work)
expt.

Fig. 5.

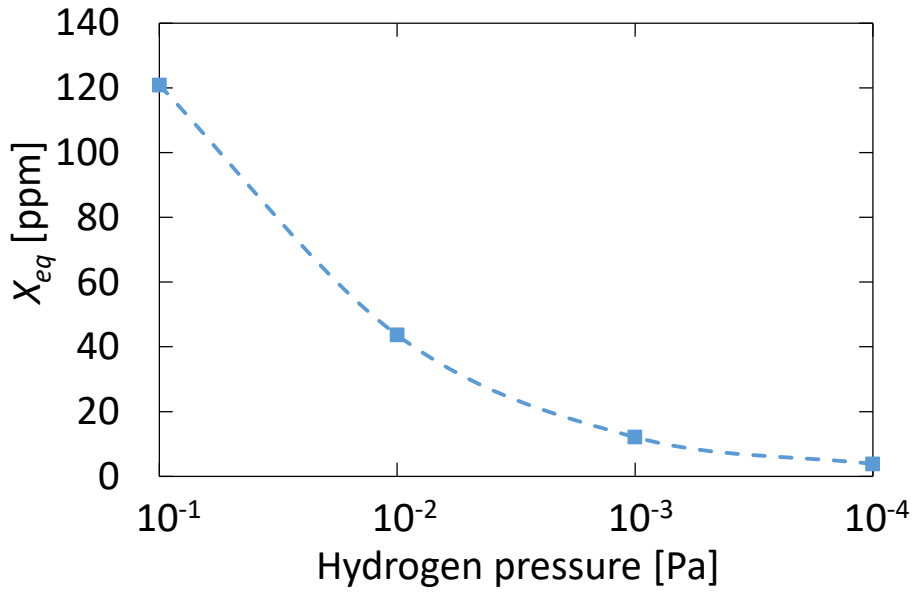
140
120
100
80
60
40
20
0
X_{eq} [ppm]
10^{-1}
10^{-2}
10^{-3}
10^{-4}
Hydrogen pressure [Pa]

Fig. 6.

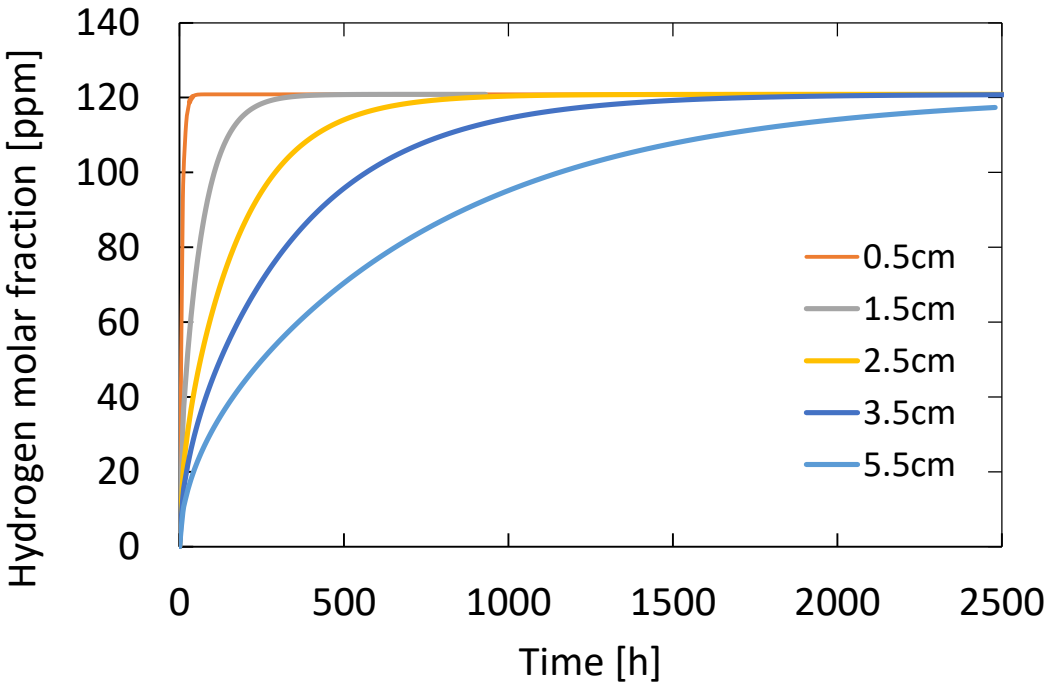
Hydrogen molar fraction [ppm]
140
120
100
80
60
40
20
0
0
500
1000
1500
2000
2500
Time [h]
0.5cm
1.5cm
2.5cm
3.5cm
5.5cm

Fig. 7.

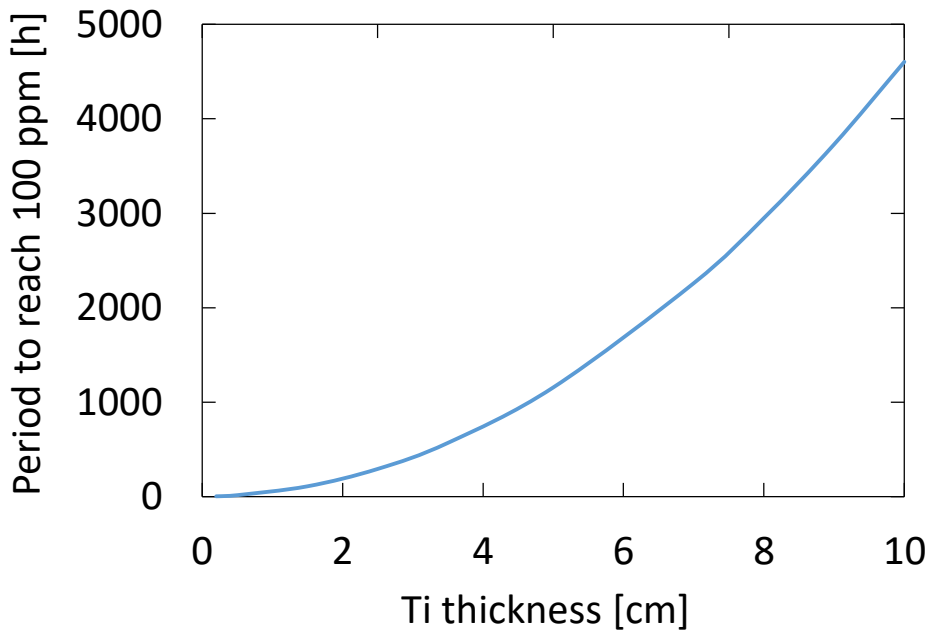
Period to reach 100 ppm [h]
5000
4000
3000
2000
1000
0
0
2
4
6
8
10
Ti thickness [cm]

Fig. 8.

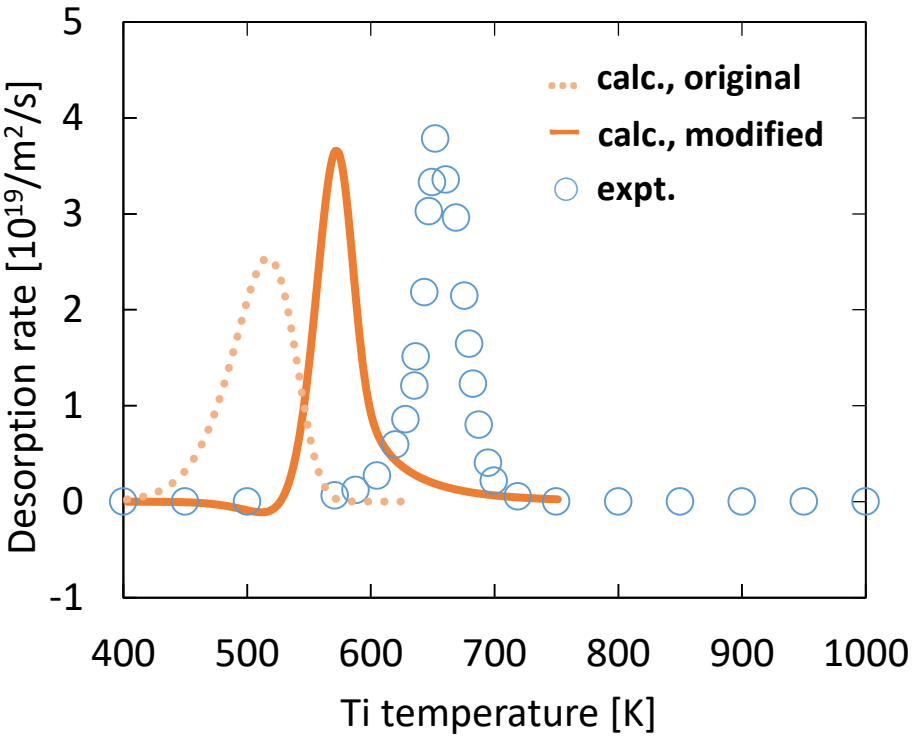
5
4
3
2
1
0
-1
Desorption rate [10^19/m^2/s]
400
500
600
700
800
900
1000
Ti temperature [K]
calc., original
calc., modified
expt.

Fig. 9.